


Recycled calcium carbonate is an efficient oxidation agent under deep upper mantle conditions

Renbiao Tao ^{1,2}✉ & Yingwei Fei ¹✉

Observations of high ferric iron content in diamond garnet inclusions and mantle plume melts suggest a highly heterogeneous distribution of ferric iron in the mantle. Recycling of oxidized materials such as carbonates from Earth's surface by subduction could explain the observed variations. Here we present high-pressure high-temperature multi-anvil experiments to determine the redox reactions between calcium-, magnesium-, or iron-carbonate and ferrous iron-bearing silicate mineral (garnet or fayalite) at conditions representative of subduction zones with intermediate thermal structures. We show that both garnet and fayalite can be oxidized to ferric iron-rich garnets accompanied by reduction of calcium carbonate to form graphite. The ferric iron content in the synthetic garnets increases with increasing pressure, and is correlated with the Ca content in the garnets. We suggest that recycled sedimentary calcium carbonate could influence the evolution of the mantle oxidation state by efficiently increasing the ferric iron content in the deep upper mantle.

¹Earth and Planets Laboratory, Carnegie Institution for Science, Washington, DC, USA. ²Present address: Center for High Pressure Science and Technology Advanced Research, Beijing, China. ✉email: rbtao@pku.edu.cn; yfei@carnegiescience.edu

Redox state (i.e., oxygen fugacity) and redox reactions affect the physical and chemical interactions between the Earth's surface and interior. In Earth's deep mantle, oxygen fugacity (fO_2) significantly affects the speciation and properties of fluids, melts, and minerals at high-pressure and high-temperature conditions^{1,2}. It has been identified for decades that Earth's subarc mantle wedge has much higher fO_2 than the oceanic mantle^{3–5}. Until now, redox evolution of subducting slab and its effect on redox state of mantle wedge is still hotly debated. The proposed oxidizing agents for the subarc mantle wedge released from subducting slabs include aqueous fluid⁶, ferric iron complexes-bearing fluid⁷, carbon- and/or sulfur-rich fluid⁸, and dissociated hydrogen from water⁹. Subducted carbonates could be an important oxidizing agent for the big mantle wedge once most of slab fluids were released at subarc mantle depth. Oceanic slabs have been seismologically observed to be subducted and deflected subhorizontally above, across, or below the 660 km discontinuity as stagnant slabs¹⁰ and form big mantle wedge¹¹. A well-studied case of big mantle wedge above a stagnant slab is formed by subduction of Pacific slab in mantle transition zone beneath eastern China¹², which may also result in the destruction of eastern North China craton¹³. Isotopic tracers show recycled carbonates by Pacific slab have metasomatized peridotite overlying mantle transition zone beneath eastern China, which become sources of Cenozoic intraplate basalts with characteristics of light Mg and Sr isotope¹⁴, heavy Zn and Fe isotope^{15,16}, and relatively oxidized and Fe-rich mantle melts^{17–19}.

The interaction between mantle minerals and the subducting materials (e.g., carbonate) may be the most important process that alters the oxidation of the deep upper mantle. Garnet is an important Fe^{3+} sink and redox index mineral in the Earth's upper mantle and transition zone once spinel becomes unstable at pressures above 2 GPa ($> \sim 60$ km)^{20,21}. Garnets in peridotite from the uppermost upper mantle contain limited Fe^{3+} content and reveal a trend of increasing $Fe^{3+}/\Sigma Fe$ ratio ($0.02 < Fe^{3+}/\Sigma Fe < 0.14$) but decreasing fO_2 from FMQ-1 to FMQ-4 with increasing depth from ~ 60 km to ~ 250 km^{22,23}. At depths > 250 km, the oxidation condition of an asthenosphere mantle is controlled below iron-wüstite (IW) buffer (i.e., $fO_2 < IW$) by (Fe, Ni) metal from disproportionation of Fe^{2+} -bearing mantle silicates²⁴. However, Kiseeva et al.²⁵ reported a series of Fe^{3+} -rich majoritic garnet ($0.08 < Fe^{3+}/\Sigma Fe < 0.30$) in diamond from the lowermost upper mantle and transition zone. The recorded fO_2 by these majoritic garnet inclusions increases from $\sim IW + 0.3$ to $\sim IW + 3$ with an increase of depth from 240 km to 500 km. Notably, Xu et al.²⁶ also reported extremely Fe^{3+} -rich majoritic garnet ($Fe^{3+}/\Sigma Fe = \sim 0.8$) inclusions in websterite xenolith, which was transported to Earth's surface by Ca-rich carbonatitic magmas from deep upper mantle or transition zone (~ 14 GPa)²⁷. In fact, calcite ($CaCO_3$), $CaSiO_3$ phase, Ca-perovskite, and $CaFe^{3+}$ -garnet inclusions have been widely reported in “super-deep” diamonds from the upper or lower mantle^{28–30}. On the other hand, mantle plume melts also show high $Fe^{3+}/\Sigma Fe$ ratio up to 0.3 and high volatile concentration (e.g., CO_2), indicating that the deep source of mantle plume is more oxidized than that associated with mid-ocean ridge and even subduction zone^{31–34}. Referring the classical model of “mantle plume from ancient oceanic crust”³⁵, recycling of oxidized materials (e.g., carbonate) from Earth's surface to deep mantle by subduction has been suggested to explain the oxidized garnet inclusions in diamond and mantle plume melt^{25,26,36}.

Carbonate is one of the important oxidized matters on Earth's surface. Previous experimental simulations have shown that metallic iron in the reduced deep mantle could be oxidized by the recycled carbonate mineral/melt at depths $> \sim 250$ km, whereas carbonate is reduced to diamond^{37–39}. Further, experimental studies also found the formation of graphite through redox

reaction between carbonate mineral/melt and wüstite (FeO) or sulfide (FeS) at upper mantle conditions^{40,41}. However, it is still unclear if the recycled carbonate can alter the ferric iron content in Fe^{2+} -bearing silicate minerals (olivine, pyroxene, or garnet), which are dominant phases in Earth's deep upper mantle. Organic matter and carbonates in sediment and altered oceanic crust are the main sources of input carbon in the subduction zones^{42,43}. Ca-carbonate ($CaCO_3$) is the most predominant carbon-bearing phase in sediments of the oceanic crust⁴³, which can be subducted into the Earth's deep upper mantle or lower mantle as a metasomatic agent for the formation of the “super-deep” diamond^{28,44,45}, although parts of them may release from slabs by dissolution \pm melting \pm amorphization during subduction^{46–48}. Pure carbonate ($CaCO_3$, $MgCO_3$, or $FeCO_3$) is known to be stable at conditions throughout Earth's upper mantle^{47,49–54}, and magnesite ($MgCO_3$) was proposed as the oxidizing agent to change redox state of deep mantle³⁶. However, as discussed above, geological observations show a possible correlation between diamond, $CaFe^{3+}$ -garnet, and Ca-carbonate, instead of Mg-carbonate. This motivates us to investigate the role of the recycled Ca-carbonate in the evolution of the redox state in the deep upper mantle.

In this study, we designed and carried out a series of high-pressure experiments to investigate the effect of the recycled carbonates on the oxidation state of the deep upper mantle. Specifically, we examine possible redox reactions between carbonate minerals ($CaCO_3$, $MgCO_3$, and $FeCO_3$) and Fe^{2+} -bearing silicate minerals (Fe^{2+} -garnet and fayalite) at high-pressure and high-temperature conditions relevant to subduction zones. The results show that only the redox reaction involving Ca-carbonate is capable of forming $CaFe^{3+}$ -garnets with $Fe^{3+}/\Sigma Fe$ ratios up to ~ 1 and graphite, providing experimental evidence for the increase of the ferric iron content in the silicates that may ultimately alter the oxidization of Earth's big mantle wedge by recycling sedimentary Ca-carbonate.

Results

We conducted seven experiments on the reaction of Fe^{2+} -garnet and $CaCO_3$ from 6 to 14 GPa and four experiments on the reaction of Fe^{2+} -garnet with $MgCO_3$ or $FeCO_3$ at 12 and 14 GPa. Further, four experiments on the reaction of fayalite (Fe_2SiO_4) and $CaCO_3$ were conducted from 3 to 12 GPa to understand the reaction mechanism, particularly the relationship between the Fe^{2+} -rich silicate and the formation of graphite during the redox reaction. All experiments were performed in a multi-anvil and a piston cylinder device. The chemical compositions of starting Fe^{2+} -garnet and fayalite are listed in Table S-1. Experimental conditions (pressure, temperature, heating duration) and run products are summarized in Table S-2. Chemical compositions of the run products for the garnet-carbonate reaction and the fayalite-carbonate reaction are listed in Supplementary Data 1 and Supplementary Data 2, respectively. A time study was carried out to evaluate reaction kinetics. Experiment (PL1395) heated at 1100 °C for 12 h produced small grain size (Fig. 1a and Fig. S-1a) and large standard deviation (σ) of the chemical analysis (Supplementary Data 1), indicating its disequilibrium. Therefore, experiments were typically heated for > 20 h to reach equilibrium.

In experiments using Fe^{2+} -garnet + $CaCO_3$ as starting materials with $CaCO_3$ in excess, Ca-carbonate (aragonite) is present in all run products (Fig. S-1). With increasing pressure, carbonate assemblages convert from pure aragonite to aragonite + dolomite, then to aragonite + magnesite (Table S-2). We also conducted an experiment with Fe^{2+} -garnet + 10 wt% $CaCO_3$ as starting material, and only magnesite was observed because of the Mg-Ca

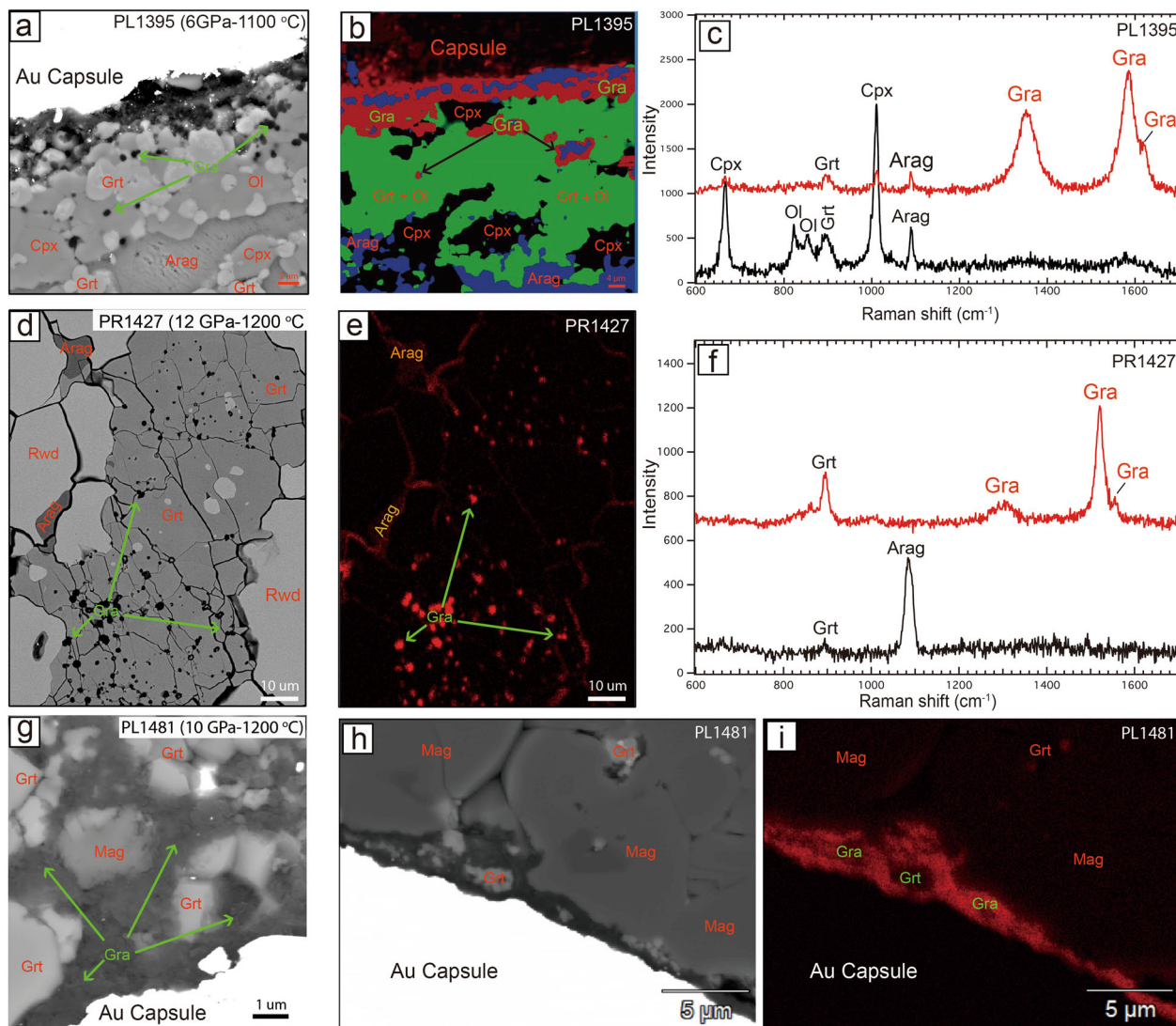


Fig. 1 Experimental products from redox reactions between Ca-carbonate and Fe^{2+} -silicates at high-pressure and high-temperature conditions. **a** BSE image of graphite (Gra)-bearing mineral assemblage of garnet (Grt), olivine (Ol), clinopyroxene (Cpx), and aragonite (Arag) in experiment between Fe^{2+} garnet and saturated CaCO_3 (PL1395). **b** Raman map confirming graphite (Gra; red)-bearing mineral assemblages consisting of garnet + olivine (Grt + Ol; Green), clinopyroxene (Cpx; black) and aragonite (Arag; blue) in PL1395. **c** Typical Raman spectrum of disordered graphite (red), aragonite, clinopyroxene (black), olivine and garnet in PL1395. **d** BSE image showing dark graphite (Gra) dots in garnet (Grt) in equilibrium with Fe-ringwoodite (Rwd) in experiment between fayalite and saturated CaCO_3 (PR1427). **e** EDS carbon elemental map showing graphite (Gra; red) dots in garnet (Grt) in PR1427. **f** Raman spectrum of partly disordered graphite (red) inclusions in garnet (Grt), and aragonite (Arag; black) in PR1427. **g, h** BSE image showing graphite (Gra), garnet (Grt), and magnesite (Mag) in experiment between Fe^{2+} garnet and 10 wt% CaCO_3 (PL1481). **i** EDS carbon elemental map, corresponding to BSE image **h**, showing graphite (Gra; red) distribution near Au capsule in PL1481.

exchange between silicate and carbonate. Silicate assemblages are predominantly composed of garnet + clinopyroxene \pm olivine. Minor spinels are also observed in PL1345 and PL1481. Notably, disordered graphite are identified by Raman spectrum, back-scatter electron (BSE) images, and energy dispersive spectroscopy (EDS) elemental map in PL1395 and PL1481, both of which are carried out in Au capsule (Fig. 1a–c, g–i). Aragonites always contain several weight percent of MgO and FeO contents, which generally decrease with experimental pressure (Supplementary Data 1). Dolomite and magnesite in the high-pressure runs contain several weight percent (up to 5.5 wt.%) of FeO contents as solid solution of dolomite-ankerite and magnesite-siderite, respectively (Supplementary Data 1).

We are particularly interested in the changes of chemical compositions of the coexisting garnets from the redox reaction between saturated Ca-carbonate and Fe^{2+} -silicates at high

pressure and high temperature. Figure 2 shows the Si (pfu), Ca (pfu), Al (pfu), and $\text{Fe}^{3+}/\Sigma\text{Fe}$ ratio in the garnets as a function of pressure. The striking feature is that the $\text{Fe}^{3+}/\Sigma\text{Fe}$ ratio in the garnets linearly increases from 0.59 at 6 GPa to almost 1.0 at 14 GPa (Fig. 2). The Si content in all garnets is centered at ~ 3.00 , indicating no majoritic substitution, contrary to the results of our previous study with a low Ca-starting material²⁷.

We also conducted two experiments at 12 and 14 GPa using Fe^{2+} -garnet and MgCO_3 as starting material. There is no evidence for redox reaction between Fe^{2+} -garnet and Mg-carbonate because the garnets contains no Fe^{3+} and no graphite is observed in both experiments (Fig. S-2a and Fig. S-4). On the other hand, the reaction between Fe^{2+} -garnet and FeCO_3 at 12 and 14 GPa produced dark graphite dots (Fig. S-2b). The $\text{Fe}^{3+}/\Sigma\text{Fe}$ ratio of the garnets ranges from 0.22 to 0.24 (Fig. S-4). The garnets from both MgCO_3 and FeCO_3 experiments contain higher Si (pfu) ranging

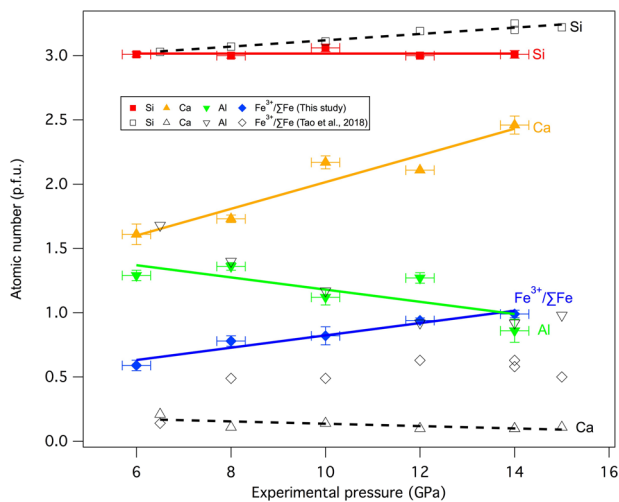


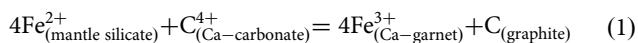
Fig. 2 Chemical composition evolution of synthetic garnets with experimental pressure in this study and comparison with that from previous study. Linear correlation between Ca, Al, Si atomic number (pfu), $\text{Fe}^{3+}/\Sigma\text{Fe}$ ratio in garnets and experimental pressure from experiments between Fe^{2+} -garnet and CaCO_3 in this study (colored symbols and lines) is compared with those from previous study with low Ca but high Fe^{3+} starting material²⁷ (black symbols and lines). Error bars for atomic number of synthetic garnets are standard deviation for multiple analyses on different garnet grains in a run product, while pressure error in our experimental range is estimated at ± 0.5 GPa for multil-anvil press.

from 3.11 to 3.21 (Supplementary Data 1), than that from CaCO_3 experiments, indicating considerable majoritic substitution.

The reduced carbon was not always observed in the Fe^{2+} -garnet- CaCO_3 experiment even with Fe^{3+} -rich garnets, which may be related to the amounts of carbon produced by the redox reaction and possible reaction of carbon with hydrogen through Pt capsule. To further investigate the formation of graphite in the system, we conducted four experiments using fayalite and CaCO_3 , which are expected to oxidize significant amounts of Fe^{2+} to Fe^{3+} in the silicates (Fig. S-3). Graphite dots were observed in all Fe^{3+} -rich products (i.e., spinel or garnet) by carbon elemental EDS map and/or Raman spectrum (Figs. 1d, 1e, and 1f; Fig. S-3). The Fe contents in aragonite generally increase from 8.22 to 30.46 wt % with an increase in pressure (Supplementary Data 2). The $\text{Fe}^{3+}/\Sigma\text{Fe}$ ratios in spinels and garnets are ranging from 0.39 to 0.65 and from 0.58 to 0.63, respectively (Supplementary Data 2). We used both “Flank method” and charge balance calculation to estimate the $\text{Fe}^{3+}/\Sigma\text{Fe}$ ratio, and both produced consistent results (Supplementary Data 3).

Discussion

Redox reactions and role of Ca in majoritic substitution. The high $\text{Fe}^{3+}/\Sigma\text{Fe}$ ratio in the garnets must be resulted from the redox reaction with CaCO_3 that should form reduced carbon and make CaO available to be incorporated in the garnet. The amounts of reduced carbon produced in the system are directly related to how much Fe^{2+} is oxidized to Fe^{3+} in the silicate. The observed graphite in the reaction of Fe^{2+} -silicate mineral (garnet or olivine) with CaCO_3 supports the proposed redox reaction. The high Ca content in the coexisting garnet is also consistent with the redox reaction that can be expressed by



A similar redox reaction has been proposed to explain the appearance of graphite and Fe^{3+} -bearing carbonate melt in the

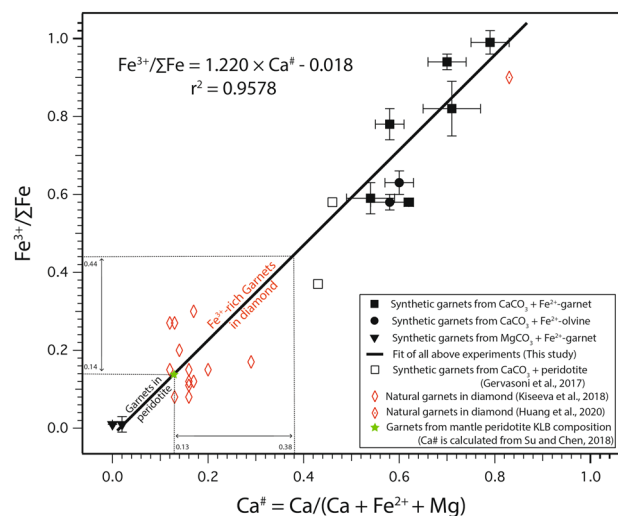
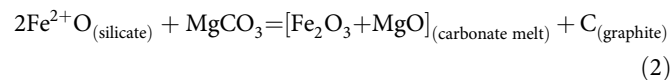


Fig. 3 Linear correlation between $\text{Fe}^{3+}/\Sigma\text{Fe}$ ratio and $\text{Ca}^\#$ in synthetic garnets from high-pressure experiments and natural garnets in diamonds. Experiments between Fe^{2+} -garnet and CaCO_3 (solid square), experiments between fayalite and CaCO_3 (solid circle), and experiments between Fe^{2+} -garnet and MgCO_3 (solid triangle) are from this study. The $\text{Ca}^\#$ of a garnet from KLB mantle peridotite (green star) was calculated from the established correlation between garnet $\text{Ca}^\#$ and $\text{CaO}/\text{Al}_2\text{O}_3$ ratio of bulk rock⁵⁸. Re-calculated chemical composition of synthetic garnets from metasomatic reaction between peridotite and saturated CaCO_3 (black square)⁵⁷ and a natural garnet inclusions in diamond from deep upper mantle (red diamond)^{25,29} are also plotted for comparison. Error bars for $\text{Fe}^{3+}/\Sigma\text{Fe}$ and $\text{Ca}^\#$ of synthetic garnets are standard deviation for multiple analyses on different garnet grains in a run product.

experimental products of carbonated peridotite at 6–10 GPa:⁵⁵



However, the CaFe^{3+} -garnet is a more efficient Fe^{3+} sink than carbonate melt because the $\text{Fe}^{3+}/\Sigma\text{Fe}$ ratio in garnet could reach one in our experiments. The formation of the CaFe^{3+} -garnet in the Ca-carbonated silicate system would be accompanied by the production of reduced carbon such as graphite/diamond in the system.

The high Fe^{3+} and Ca content in garnet has a unique effect on the majoritic component as a function of pressure. The priority substitution is $\text{Mg}^{2+} + \text{Al}^{3+} = \text{Ca}^{2+} + \text{Fe}^{3+}$ in the CaFe^{3+} -garnet, instead of the pressure-dependent majoritic substitution of $\text{Al}^{3+} + \text{Al}^{3+} = \text{Mg}^{2+} + \text{Si}^{4+}$. Therefore, there is no excess Si in garnets at high pressure. However, Ca (pfu) and Al (pfu) in the garnets linearly increase or decrease with pressure, respectively (Fig. 2), which can be used as a garnet geobarometer for the Ca-rich garnets. It is noted that the garnets after experiments contain the Al_2O_3 content (~ 15 wt.%) between the starting composition (7.11 wt.%) and regular garnet, which is balanced by the amounts of Fe^{3+} formed in the system. The competition to occupy the site by Al^{3+} and Fe^{3+} in garnets is controlled by their thermodynamical stability⁵⁶. The increase of the Al_2O_3 content in the resulted garnets relative to that of the starting material led to the presence of other silicate such as Cpx in the run product, instead of a single garnet phase.

Oxidization of big mantle wedge and formation of CaFe^{3+} -garnet in diamond. Figure 3 shows an excellent linear correlation (black line) between the $\text{Fe}^{3+}/\Sigma\text{Fe}$ ratio and $\text{Ca}^\#$ in the synthetic garnets from our experiments. The $\text{Fe}^{3+}/\Sigma\text{Fe}$ ratio of the garnet is

well controlled by the $\text{Ca}^\#$ of garnet:

$$\text{Fe}^{3+}/\sum\text{Fe} = 1.220 \times \text{Ca}^\# - 0.018 \quad (3)$$

Chemical compositions of garnets from metasomatic reaction between peridotite and CaCO_3 in previous study (black square)⁵⁷ and CaFe^{3+} -rich garnet inclusions in natural diamond from the deep upper mantle (red diamond)^{25,29} are also consistently plotted on the fitted line (Fig. 3), indicating equation (3) can be applied to natural metasomatism of mantle peridotite by the recycled Ca-carbonate in the deep upper mantle.

Recently, Su and Chen⁵⁸ established the correlation between the $\text{Ca}^\#$ of garnet and the $\text{CaO}/\text{Al}_2\text{O}_3$ ratio of bulk rock for mantle peridotite system, which can be used to calculate the $\text{Ca}^\#$ of a garnet formed in an unmetasomatic mantle peridotite. For a KLB mantle composition⁵⁹, the $\text{Ca}^\#$ of garnet is calculated at 0.13, corresponding to the $\text{Fe}^{3+}/\sum\text{Fe}$ ratio of 0.14 by equation (3) (green star in Fig. 3). This is consistent with that of the natural garnets in peridotite from the uppermost upper mantle with the $\text{Fe}^{3+}/\sum\text{Fe}$ ratio increasing from 0.02 to 0.14 with increase depth from ~80 to ~250 km^{22,23}. In other words, all garnets formed in an unmetasomatic mantle peridotite should have low $\text{Ca}^\#$ (<0.13) and low $\text{Fe}^{3+}/\sum\text{Fe}$ ratio (<0.14) at same time. The observed $\text{Fe}^{3+}/\sum\text{Fe}$ ratio and $\text{Ca}^\#$ of the CaFe^{3+} -garnets in diamonds from the deep upper mantle and transition zone^{25,29,60} range from 0.14 to 0.40 and from 0.13 to 0.38, respectively (Fig. 3 and Fig. S-4). These garnets with high $\text{Ca}^\#$ and high $\text{Fe}^{3+}/\sum\text{Fe}$ ratio must be associated with mantle rocks having high $\text{CaO}/\text{Al}_2\text{O}_3$. The recycling of sedimentary Ca-carbonate (marble) along a subducting slab is the best candidate to introduce high $\text{CaO}/\text{Al}_2\text{O}_3$ material because the sedimentary Ca-carbonate has a high $\text{CaO}/\text{Al}_2\text{O}_3$ ratio⁶¹. Both pressure and the $\text{Ca}^\#$ have a positive effect on the $\text{Fe}^{3+}/\sum\text{Fe}$ ratio in the garnets.

The silicate starting materials (Fe^{2+} -garnet and fayalite) used in this study are free of Fe^{3+} . After reacting with Ca-carbonate (CaCO_3) at high pressure and high temperature, significant amounts of Fe^{3+} -rich garnet are produced. The proposed redox reaction should also reduce some carbonate to graphite/diamond. Graphites are clearly identified in all experiments with the CaCO_3 and fayalite reaction and also in two experiments (PL1395 and PL1481) with the CaCO_3 and Fe^{2+} -garnet reaction. All experiments with identified graphite were performed in gold (Au) capsule (Table S-2). However, no graphite was identified in other experiments with the CaCO_3 and Fe^{2+} -garnet reaction in platinum (Pt) capsule, although more Fe^{3+} -rich garnets were produced at high pressure. Typically graphite produced by the reaction migrates to the Au capsule interface, even into the capsule (Fig. S-5). It is likely that the loss of the reduced carbon in the experiments with Pt capsule is related to hydrogen diffusion into the Pt capsule at high temperature, as demonstrated by ¹³C solid-state NMR analysis of the synthetic samples from high-pressure experiments⁶². In addition, the amounts of graphite produced in the run product are very small (0.07–0.13 volume%) by mass balance calculations according to equation (1), considering oxidation of 22–37 volume % garnets (See method part and Table S-3), that could make the detection of graphite more challenge.

Although the experiments were performed in the diamond stability field, we have only observed graphite in the run products because of a large kinetic barrier for the conversion from graphite to diamond⁶³. Significant over-pressure is required to form diamond without metal catalyst in laboratory experiments. We infer diamond formation based on the known equilibrium boundary of the graphite–diamond conversion. In the natural process, we expect that all observed graphite in the diamond stability field should be diamond under deep mantle conditions.

Our experimental results show that the redox reaction prefers to occur between Fe^{2+} -rich mantle rock and Ca-carbonate to produce CaFe^{3+} -rich garnet and reduced carbon (graphite). At 14 GPa, corresponding to conditions near the transition zone, the $\text{Fe}^{3+}/\sum\text{Fe}$ ratio of garnets in the CaCO_3 -saturated system is close to 1. For natural garnets in diamond (Fig. S-4), the highest $\text{Fe}^{3+}/\sum\text{Fe}$ ratio is ~0.3 at ~14 GPa²⁵. Considering the molar ratio of oxidant (C^{4+} to C^0) and reductant (Fe^{2+} to Fe^{3+}) in the redox reaction (1), we estimated that 7.5% mole percent sedimentary CaCO_3 in the recycled oceanic crust is sufficient to produce an $\text{Fe}^{3+}/\sum\text{Fe}$ ratio of 0.3 in the garnet at deep upper mantle condition, suggesting that the recycled Ca-carbonate is an efficient agent to elevate the Fe^{3+} content in the Earth's upper mantle through geological time.

The major source of the recycled Ca-carbonate in the subduction zone is sedimentary carbonate in the oceanic crust⁴². Figure 4 illustrates that the potential influence of the recycled-sedimentary Ca-carbonate on the big Earth's mantle wedge through the proposed redox reaction. Any CaFe^{3+} -garnet found in diamond or Fe^{3+} -rich mantle melt from the deep upper mantle would be an indicative signature from the recycled-sedimentary Ca-carbonates because of the redox reaction. Taking the big mantle wedge beneath eastern China formed by subduction of Pacific slab⁶⁴ as an example, melting of carbonated peridotites by metasomatism of the recycled Ca-carbonate in the big mantle wedge could be the sources of Cenozoic basalts with the characteristic of oxidized and Fe-rich mantle melts^{17–19}, light Mg, Sr isotope^{64,65}, and heavy Zn, Fe isotope^{15,16}. “Super-deep” diamonds from deep upper mantle or transition zone also need an introduction of a metasomatic agent such as sedimentary CaCO_3 of the recycled oceanic crusts^{28,44,45}, but the CaCO_3 component has to be undersaturated in order to account for the observed Ca content in the silicates. In other case, mantle plume melt with a high $\text{Fe}^{3+}/\sum\text{Fe}$ ratio and high volatiles (e.g., CO_2) may also be derived from the deep upper mantle with a CaFe^{3+} -garnet source produced by the recycled-sedimentary Ca-carbonates^{31–34}. Our experimental results on the coupled formation of reduced carbon and Fe^{3+} -rich silicate illustrate the importance of the recycled-sedimentary Ca-carbonates for the evolution of the redox state and carbon cycling in the deep upper mantle.

Method

High-pressure experimental synthesis. The chemical composition of Fe^{2+} -garnet is analogous to that of natural Fe^{3+} -rich majoritic garnet in websterite xenolith from Earth's deep upper mantle²⁶. In addition, fayalite is used to react with CaCO_3 to understand the reaction mechanism in a simplified CaO-FeO-SiO₂-CO₂ system. Silicate starting materials (Fe^{2+} -garnet or fayalite) were reduced in gas-mixing furnace under controlled $f\text{O}_2$ at ~IW buffer by mixing different flux of CO₂ and H₂ gas at high temperature (1100 °C). Powder X-ray diffraction shows no Fe^{3+} -bearing phases in synthetic Fe^{2+} garnet and fayalite. The chemical compositions of Fe^{2+} -garnet and fayalite are listed in Table S-1. In comparison with that of oceanic crust⁶⁶, Martian silicate⁶⁷ and Earth's mantle⁵⁹, chemical composition of Fe^{2+} -garnet in this study is similar with that of Martian silicate, which contains higher FeO content than Earth's mantle, but lower Al₂O₃ content than oceanic crust (Table S-1). Carbonate starting materials used in this study are CaCO_3 (99.99% pure, Alfa Aesar Company), MgCO_3 (99.9% pure, Scholar chemistry Company), natural siderite ($\text{Fe}_{0.950}\text{Mn}_{0.046}\text{Mg}_{0.004}\text{CO}_3$; Ivigtut, Greenland)⁴⁹, respectively. In order to simulate geological metasomatic process occurring on slab-mantle surface in subduction zones, in most case, silicate starting materials were sandwiched by saturated carbonates (CaCO_3 , or MgCO_3 , or FeCO_3) in Au or Pt capsules, respectively. In some experiments, silicate and carbonates are homogeneously mixed to promote efficiency of the redox reaction (Table S-2). All high-pressure experiments are conducted at Geophysical Laboratory of Carnegie Institution for Science. Experiment at 3 GPa is carried out in a well-calibrated end-loaded piston cylinder⁶⁸. All other experiments from 6 to 14 GPa are carried out in a multi-anvil apparatus by using 14/8-type assemblage, which is well calibrated⁶⁹. A type-C thermocouple, inserted axially to top of the capsule, is used to measure experimental temperature for piston cylinder and multi-anvil experiments. Pressures and temperatures were automatically controlled through computer program. To simulate intermediate geothermal condition in subduction zones, experimental temperatures are lower than normal mantle geotherm, ranging from 900 °C to

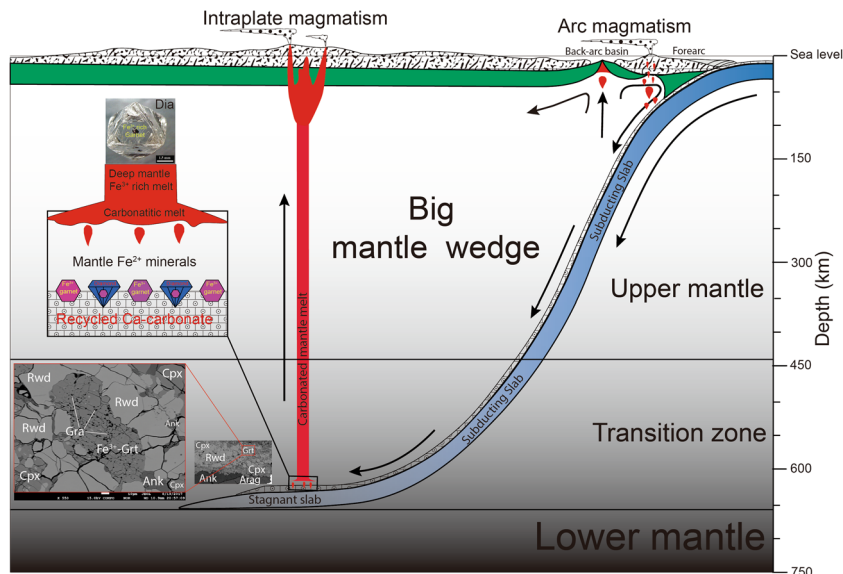


Fig. 4 Geological model of oxidation of deep upper mantle by recycled-sedimentary Ca-carbonate. Cartoon illustrates the formation of CaFe^{3+} -garnet in diamond and Fe^{3+} -rich carbonated melt from redox reaction between mantle Fe^{2+} -silicate and recycled-sedimentary Ca-carbonate in big mantle wedge. Image of diamond with a Fe^{3+} -rich garnet inclusion is from Wood et al.²¹.

1300 °C (Table S-2). After experiments, powder supply to the furnace is shut off to quickly quench experiments.

Analysis of synthetic samples. The recovered samples are mounted in epoxy resin, and polished with aluminum oxide powder (<1 μm) for measurements by Raman spectroscopy and electron probe microanalyzer. Raman spectra from 200 to 1500 cm^{-1} were collected using a confocal micro-Raman spectroscopy (JASCO NRS-3100; 514.5 nm Ar-ion laser) at Geophysical Laboratory. Raman map on one sample (PL1395) with high-graphite contents was collected on a confocal LabRam HR800 spectrometer (Horiba Jobin-Yvon) of 800 mm focal length equipped with a 532 nm Nd:YAG laser and a Mitutoyo 50 long working distance objective (0.42 NA) at Ecole Normale Supérieure de Lyon, France. Raman spectra for a map are acquired between 300 cm^{-1} and 1800 cm^{-1} with a spectral resolution of 0.3 cm^{-1} . BSE images, elemental mapping from the EDS and chemical composition analysis are obtained by JEOL JXA-8530F Field Emission electron probe at Geophysical laboratory using appropriate silicate standards, a beam current of 30 nA and a 15 kV voltage with conventional ZAF data reduction techniques. Chemical compositions for each phase are derived from multi-analysis, and standard deviation (σ) for multi-analysis are calculated as analytical error. Chemical formulas and $\text{Fe}^{3+}/\Sigma\text{Fe}$ ratio for each phase were calculated based on charge balance⁷⁰. “Flank method” on electron probe is also applied to measure the $\text{Fe}^{3+}/\Sigma\text{Fe}$ ratio of some synthetic garnets in comparison with charge balance method (Supplementary Data 3), following the calibration and measurement procedure described in our previous study²⁷.

Mass balance calculation of graphite production. The area ratio of synthetic garnets in run products are measured on BSE images using the ImageJ software⁷¹. Molar volumes of garnet endmembers and graphite are from an updated thermodynamic database⁷². Based on area ratio and chemical compositions of synthetic garnets from different experiments, the molar mass of Fe^{3+} content in garnets can be calculated. According to molar ratio between Fe^{3+} and C (1:4) in redox reaction between Ca-carbonate and mantle Fe^{2+} rock: $4\text{Fe}_{(\text{mantle mineral})}^{2+} + \text{C}_{(\text{Ca-carbonate})}^{4+} = 4\text{Fe}_{(\text{Ca-rich garnet})}^{3+} + \text{C}_{(\text{graphite})}$, the molar mass and area ratio of graphite in the run product in this study is calculated (Table S-3).

Comparison of $\text{Fe}^{3+}/\Sigma\text{Fe}$ ratios and $\text{Ca}^\#$ in synthetic and natural garnets. McCammon and Ross⁷³ found the relative concentration of Fe^{3+} in synthetic $\text{Mg}(\text{Fe}(\text{Si},\text{Al})\text{O}_3)$ garnets increases both with total iron content and increasing oxygen fugacity, but not with Al concentration. Although very-oxidized Re- ReO_2 buffer was used in their study, the highest $\text{Fe}^{3+}/\Sigma\text{Fe}$ ratio for the synthetic majoritic garnets is still <0.22. In Figure S-4, we plotted $\text{Fe}^{3+}/\Sigma\text{Fe}$ ratio and $\text{Ca}^\#$ [i.e., $\text{Ca}/(\text{Ca} + \text{Mg} + \text{Fe}^{2+} + \text{Mn})$] of synthetic garnets in this study and previous study²⁷, and natural garnets in diamond^{25,60}, mantle xenolith²⁶, and shocked meteorite^{13,27}. It clearly shows that there are two evolution series: low Ca but high Fe^{3+} series; High Ca and high Fe^{3+} series. Along both series, the $\text{Fe}^{3+}/\Sigma\text{Fe}$ ratio of garnets can evolve from 0 to ~1 with increase of pressure.

Along the low Ca series, if $\text{MgO} \pm \text{CO}_2$ in the system is in excess, which is the case of experiments between Fe^{2+} -garnet and MgCO_3 in this study, $\text{Fe}^{3+}/\Sigma\text{Fe}$ ratios

of synthetic garnets are very low (<0.02). Synthetic garnets may evolve to pyrope ($\text{Mg}_3\text{Al}_2\text{Si}_3\text{O}_{12}$) endmember (Figure S-4). If all Fe is introduced in system by Fe^{3+} , which is the case of synthetic garnets from Fe^{3+} -rich composition in our previous study²⁷, $\text{Fe}^{3+}/\Sigma\text{Fe}$ ratios of synthetic garnets are increasing with increase of experimental pressure. The synthetic garnets may evolve to khorharite endmember ($\text{Mg}_3\text{Fe}^{3+}_2\text{Si}_3\text{O}_{12}$) (Figure S-4), which is a rare garnet endmember and only reported in majoritic garnets from shocked meteorite⁷⁴. Indeed, we do find chemical compositions of all majoritic garnets from shocked meteorite^{13,27} are plotted on this evolution series (Figure S-4). The formation of garnets on this series requires very special conditions: high Mg, high Fe^{3+} but low Ca contents in system, and high pressure. Geologically, the shocking process of meteorite may be able to provide the right conditions for them. The high Fe^{3+} content may be formed from disproportionation at extremely high-pressure condition during shock process⁷⁵. Notably, chemical compositions of majoritic garnets from mantle xenolith¹ are also plotted on this series (Figure S-4). If $\text{FeO} \pm \text{CO}_2$ in the system is in excess, which is the case of experiments between Fe^{2+} -garnet and FeCO_3 in this study, $\text{Fe}^{3+}/\Sigma\text{Fe}$ ratios of synthetic garnets are still low, ranging from 0.22 to 0.24, and synthetic garnets may evolve to skiaigite endmember ($\text{Fe}_3\text{Fe}^{3+}_2\text{Si}_3\text{O}_{12}$) (Figure S-4). A possible redox reaction between Fe^{2+} -garnet and Fe-carbonate may occur in this system and result in the formation of reduced graphite and skiaigite garnet at same time.

Data availability

All data used in the study can be accessed in supplementary material online. Data are also available on Mendeley Data repository at <https://doi.org/10.17632/2g42x8gvp2.4>.

Received: 23 June 2020; Accepted: 28 January 2021;

Published online: 23 February 2021

References

- Frost, D. J. & McCammon, C. A. The redox state of Earth’s mantle. *Annu. Rev. Earth Planet. Sci.* **36**, 389–420 (2008).
- Stagno, V. & Fei, Y. The Redox boundaries of Earth’s interior. *Elements* **16**, 167–172 (2020).
- Evans, K. A., Elburg, M. A. & Kamenetsky, V. S. Oxidation state of subarc mantle. *Geology* **40**, 783–786 (2012).
- Parkinson, I. J. & Arculus, R. J. The redox state of subduction zones: insights from arc-peridotites. *Chem. Geol.* **160**, 409–423 (1999).
- Wood, B. J. & Virgo, D. Upper mantle oxidation state: Ferric iron contents of lherzolite spinels by ⁵⁷Fe Mössbauer spectroscopy and resultant oxygen fugacities. *Geochem. Cosmochim. Acta* **53**, 1277–1291 (1989).
- Kelley, K. A. & Cottrell, E. Water and the oxidation state of subduction zone magmas. *Science* **325**, 605–607 (2009).
- Debret, B. et al. Redox transfer at subduction zones: insights from Fe isotopes in the Mariana forearc. *Geochem. Persp. Lett.* **12**, 46–51 (2020).

8. Rielli, A. et al. Evidence of sub-arc mantle oxidation by sulphur and carbon. *Geochem. Persp. Lett.* **3**, 124–132 (2017).
9. Tollan, P. Arc magmas oxidized by water dissociation and hydrogen incorporation in orthopyroxene. *Nat. Geosci.* **12**, 667–671 (2019).
10. Fukao, Y., Widiyantoro, S. & Obayashi, M. Stagnant slabs in the upper and lower mantle transition region. *Rev. Geophys.* **39**, 291–323 (2001).
11. Maruyama, S. et al. The dynamics of big mantle wedge, magma factory, and metamorphic–metasomatic factory in subduction zones. *Gondwana Res.* **16**, 414–430 (2009).
12. Huang, J. & Zhao, D. High-resolution mantle tomography of China and surrounding regions. *J. Geophys. Res. Solid Earth* **111**, B09305 (2006).
13. Zhu, R. et al. Destruction of the North China Craton. *Sci. China Earth Sci.* **55**, 1565–1587 (2012).
14. Li, S.-G. et al. Deep carbon cycles constrained by a large-scale mantle Mg isotope anomaly in eastern China. *Natl. Sci. Rev.* **4**, 111–120 (2016).
15. He, Y. et al. A nephelinitic component with unusual $\delta^{56}\text{Fe}$ in Cenozoic basalts from eastern China and its implications for deep oxygen cycle. *Earth Planet. Sci. Lett.* **512**, 175–183 (2019).
16. Liu, S.-A., Wang, Z.-Z., Li, S.-G., Huang, J. & Yang, W. Zinc isotope evidence for a large-scale carbonated mantle beneath eastern China. *Earth Planet. Sci. Lett.* **444**, 169–178 (2016).
17. Erdmann, S., Chen, L.-H., Liu, J.-Q., Xue, X.-Q. & Wang, X.-J. Hot, volatile-poor, and oxidized magmatism above the stagnant Pacific plate in Eastern China in the Cenozoic. *Geochem. Geophys. Geosyst.* **20**, 4849–4868 (2019).
18. He, D., Liu, Y., Chen, C., Foley, S. F. & Ducea, M. N. Oxidation of the mantle caused by sediment recycling may contribute to the formation of iron-rich mantle melts. *Sci. Bull.* **65**, 519–521 (2020).
19. Hong, L., Xu, Y.-G., Zhang, L., Wang, Y. & Ma, L. Recycled carbonate-induced oxidation of the convective mantle beneath Jiaodong, Eastern China. *Lithos* **273**, 35–45 (2020).
20. Robinson, J. A. C. & Wood, B. J. The depth of the spinel to garnet transition at the peridotite solidus. *Earth Planet. Sci. Lett.* **164**, 277–284 (1998).
21. Wood, B. J., Kiseeva, E. S. & Matzen, A. K. Garnet in the Earth’s Mantle. *Elements* **9**, 421–426 (2013).
22. Luth, R. W., Virgo, D., Boyd, F. R. & Wood, B. J. Ferric iron in mantle-derived garnets: Implications for thermobarometry and for the oxidation state of the mantle. *Contr. Mineral. Petrol.* **104**, 56–72 (1990).
23. Woodland, A. B. & Koch, M. Variation in oxygen fugacity with depth in the upper mantle beneath the Kaapvaal craton, Southern Africa. *Earth Planet. Sci. Lett.* **214**, 295–310 (2003).
24. Rohrbach, A. et al. Metal saturation in the upper mantle. *Nature* **449**, 456–458 (2007).
25. Kiseeva, E. S. et al. Oxidized iron in garnets from the mantle transition zone. *Nat. Geosci.* **11**, 144–147 (2018).
26. Xu, C. et al. Recovery of an oxidized majorite inclusion from Earth’s deep asthenosphere. *Sci. Adv.* **3**, e1601589 (2017).
27. Tao, R., Fei, Y., Bullock, E. S., Xu, C. & Zhang, L. Experimental investigation of Fe^{3+} -rich majoritic garnet and its effect on majorite geobarometer. *Geochim. Cosmochim. Acta* **225**, 1–16 (2018).
28. Kaminsky, F. Mineralogy of the lower mantle: a review of ‘super-deep’ mineral inclusions in diamond. *Earth Sci. Rev.* **110**, 127–147 (2012).
29. Huang, S. et al. HIMU geochemical signature originating from the transition zone. *Earth Planet. Sci. Lett.* **542**, 116323 (2020).
30. Nestola, F. et al. CaSiO_3 perovskite in diamond indicates the recycling of oceanic crust into the lower mantle. *Nature* **555**, 237–241 (2018).
31. Brounce, M., Stolper, E. & Eiler, J. Redox variations in Mauna Kea lavas, the oxygen fugacity of the Hawaiian plume, and the role of volcanic gases in Earth’s oxygenation. *Proc. Natl Acad. Sci. USA* **114**, 8997–9002 (2017).
32. Hartley, M. E., Shorttle, O., MacLennan, J., Moussallam, Y. & Edmonds, M. Olivine-hosted melt inclusions as an archive of redox heterogeneity in magmatic systems. *Earth Planet. Sci. Lett.* **479**, 192–205 (2017).
33. Mazza, S. E. et al. Sampling the volatile-rich transition zone beneath Bermuda. *Nature* **569**, 398–403 (2019).
34. Moussallam, Y. et al. Mantle plumes are oxidised. *Earth Planet. Sci. Lett.* **527**, 115798 (2019).
35. Hofmann, A. W. & White, W. M. Mantle plumes from ancient oceanic crust. *Earth Planet. Sci. Lett.* **57**, 421–436 (1982).
36. McCammon, C. A. Mantle oxidation state and oxygen fugacity: Constraints on mantle chemistry, structure, and dynamics. in *Geophysical Monograph Series* (eds. van der Hilst, R. D., Bass, J. D., Matas, J. & Trampert, J.) vol. 160, 219–240 (American Geophysical Union, 2005).
37. Palyanov, Y. N. et al. Mantle-slab interaction and redox mechanism of diamond formation. *Proc. Natl Acad. Sci.* **110**, 20408–20413 (2013).
38. Rohrbach, A. & Schmidt, M. W. Redox freezing and melting in the Earth’s deep mantle resulting from carbon–iron redox coupling. *Nature* **472**, 209–212 (2011).
39. Dorfman, S. M. et al. Carbonate stability in the reduced lower mantle. *Earth Planet. Sci. Lett.* **489**, 84–91 (2018).
40. Bataleva, Y. V., Palyanov, Y. N., Borzdov, Y. M., Kupriyanov, I. N. & Sokol, A. G. Synthesis of diamonds with mineral, fluid and melt inclusions. *Lithos* **265**, 292–303 (2016).
41. Bataleva, Palyanov, Borzdov & Bayukov Processes and conditions of the origin for Fe^{3+} -bearing magnesiowüstite under lithospheric mantle pressures and temperatures. *Minerals* **9**, 474 (2019).
42. Plank, T. & Manning, C. E. Subducting carbon. *Nature* **574**, 343–352 (2019).
43. Clift, P. D. A revised budget for Cenozoic sedimentary carbon subduction. *Rev. Geophys.* **55**, 97–125 (2017).
44. Timmerman, S. et al. Primordial and recycled helium isotope signatures in the mantle transition zone. *Science* **365**, 692–694 (2019).
45. Walter, M. J. et al. Deep mantle cycling of oceanic crust: evidence from diamonds and their mineral inclusions. *Science* **334**, 54–57 (2011).
46. Ague, J. J. & Nicolescu, S. Carbon dioxide released from subduction zones by fluid-mediated reactions. *Nat. Geosci.* **7**, 355–360 (2014).
47. Hou, M. et al. Temperature-induced amorphization in CaCO_3 at high pressure and implications for recycled CaCO_3 in subduction zones. *Nat. Commun.* **10**, 1963 (2019).
48. Poli, S. Carbon mobilized at shallow depths in subduction zones by carbonatitic liquids. *Nat. Geosci.* **8**, 633–636 (2015).
49. Tao, R., Fei, Y. & Zhang, L. Experimental determination of siderite stability at high pressure. *Am. Mineral.* **98**, 1565–1572 (2013).
50. Kang, N., Schmidt, M. W., Poli, S., Franzolin, E. & Connolly, J. A. D. Melting of siderite to 20 GPa and thermodynamic properties of FeCO_3 -melt. *Chem. Geol.* **400**, 34–43 (2015).
51. Isshiki, M. et al. Stability of magnesite and its high-pressure form in the lowermost mantle. *Nature* **427**, 60–63 (2004).
52. Cerantola, V. et al. Stability of iron-bearing carbonates in the deep Earth’s interior. *Nat. Commun.* **8**, 15960 (2017).
53. Fiquet, G. et al. Structural refinements of magnesite at very high pressure. *Am. Mineral.* **87**, 1261–1265 (2002).
54. Boulard, E. et al. Transformations and decomposition of MnCO_3 at Earth’s lower mantle conditions. *Front. Earth Sci.* **4**, 107 (2016).
55. Brey, G. P., Bulatov, V. K., Gurnis, A. V. & Lahaye, Y. Experimental melting of carbonated peridotite at 6–10 GPa. *J. Petrol.* **49**, 797–821 (2008).
56. Woodland, A. B. & O’Neill, H. S. C. Synthesis and stability of $\text{Fe}^{2+}_3\text{Fe}^{3+}_2\text{Si}_3\text{O}_{12}$ garnet and phase relations with $\text{Fe}^{2+}_3\text{Al}_2\text{Si}_3\text{O}_{12}$ - $\text{Fe}^{2+}_3\text{Fe}^{3+}_2\text{Si}_3\text{O}_{12}$ solutions. *Am. Mineralogist* **78**, 1002–1005 (1993).
57. Gervasoni, F., Klemme, S., Rohrbach, A., Grützner, T. & Berndt, J. Experimental constraints on mantle metasomatism caused by silicate and carbonate melts. *Lithos* **282–283**, 173–186 (2017).
58. Su, B. & Chen, Y. Making cratonic lithospheric mantle. *J. Geophys. Res. Solid Earth* **123**, 7688–7706 (2018).
59. Takahashi, E. Melting of a dry peridotite KLB-1 up to 14 GPa: Implications on the origin of peridotitic upper mantle. *J. Geophys. Res.* **91**, 9367 (1986).
60. Collerson, K. D. et al. Majoritic garnet: a new approach to pressure estimation of shock events in meteorites and the encapsulation of sub-lithospheric inclusions in diamond. *Geochim. Cosmochim. Acta* **74**, 5939–5957 (2010).
61. Tao, R., Zhang, L., Li, S., Zhu, J. & Ke, S. Significant contrast in the Mg-C-O isotopes of carbonate between carbonated eclogite and marble from the S.W. Tianshan UHP subduction zone: evidence for two sources of recycled carbon. *Chem. Geol.* **483**, 65–77 (2018).
62. Kim, E. J., Fei, Y. & Lee, S. K. Probing carbon-bearing species and CO_2 inclusions in amorphous carbon-MgSiO₃ enstatite reaction products at 1.5 GPa: Insights from ¹³C high-resolution solid-state NMR. *Am. Mineral.* **101**, 1113–1124 (2016).
63. Sung, J. Graphite - diamond transition under high pressure: a kinetics approach. *J. Mater. Sci.* **35**, 6041–6054 (2000).
64. Li, S. & Wang, Y. Formation time of the big mantle wedge beneath eastern China and a new lithospheric thinning mechanism of the North China craton —geodynamic effects of deep recycled carbon. *Sci. China Earth Sci.* **61**, 853–868 (2018).
65. Yang, W., Teng, F.-Z., Zhang, H.-F. & Li, S.-G. Magnesium isotopic systematics of continental basalts from the North China craton: Implications for tracing subducted carbonate in the mantle. *Chem. Geol.* **328**, 185–194 (2012).
66. White, W. M. & Klein, E. M. Composition of the oceanic crust. *Treatise Geochem.* **3**, 1–4964 (2014).
67. Taylor, G. J. The bulk composition of Mars. *Geochemistry* **73**, 401–420 (2013).
68. Boyd, F. R. & England, J. L. Apparatus for phase-equilibrium measurements at pressures up to 50 kilobars and temperatures up to 1750 °C. *J. Geophys. Res.* **65**, 741–748 (1960).
69. Bennett, N. R., Brenan, J. M. & Fei, Y. Thermometry of the magma ocean: controls on the metal–silicate partitioning of gold. *Geochim. Cosmochim. Acta* **184**, 173–192 (2016).
70. Droop, G. T. R. A general equation for estimating Fe^{3+} concentration in ferromagnesian silicates and oxides from microprobe analyses, using stoichiometric criteria. *Mineral. Magazine* **51**, 431–435 (1987).

71. Rueden, C. T. et al. ImageJ2: ImageJ for the next generation of scientific image data. *BMC Bioinform.* **18**, 529 (2017).
72. Holland, T. J. B. & Powell, R. An improved and extended internally consistent thermodynamic dataset for phases of petrological interest, involving a new equation of state for solids. *J. Metamorph. Geol.* **29**, 333–383 (2011).
73. McCammon, C. A. & Ross, N. L. Crystal chemistry of ferric iron in (Mg,Fe)(Si,Al)O₃ majorite with implications for the transition zone. *Phys. Chem. Miner.* **30**, 206–216 (2003).
74. Mason, B., Nelen, J., John, S. & White, J. R. Olivine-garnet transformation in a meteorite. *Science* **160**, 66–67 (1968).
75. Frost, D. J. et al. Experimental evidence for the existence of iron-rich metal in the Earth's lower mantle. *Nature* **428**, 409–412 (2004).

Acknowledgements

This work was supported by the National Science Foundation (grants EAR-1447311 and EAR-1619868 to Y.F.) and National Key Research and Development Program of China (2019YFA0708501 to R.T.). We thank Bjorn Mysen for helping with the Raman and Jing Yang for additional electron microprobe analysis.

Author contributions

R.T. and Y.F. initiated the project. R.T. conducted the experiments, prepared the original draft under the supervision of Y.F.

Competing interests

The authors declare no competing interests.

Additional information

Supplementary information The online version contains supplementary material available at <https://doi.org/10.1038/s43247-021-00116-8>.

Correspondence and requests for materials should be addressed to R.T. or Y.F.

Peer review information Primary handling editor: Joe Aslin

Reprints and permission information is available at <http://www.nature.com/reprints>

Publisher's note Springer Nature remains neutral with regard to jurisdictional claims in published maps and institutional affiliations.



Open Access This article is licensed under a Creative Commons Attribution 4.0 International License, which permits use, sharing, adaptation, distribution and reproduction in any medium or format, as long as you give appropriate credit to the original author(s) and the source, provide a link to the Creative Commons license, and indicate if changes were made. The images or other third party material in this article are included in the article's Creative Commons license, unless indicated otherwise in a credit line to the material. If material is not included in the article's Creative Commons license and your intended use is not permitted by statutory regulation or exceeds the permitted use, you will need to obtain permission directly from the copyright holder. To view a copy of this license, visit <http://creativecommons.org/licenses/by/4.0/>.

© The Author(s) 2021